Emergent geometry from random multitrace matrix models

B. Ydri,[*] A. Rouag, and K. Ramda

Department of Physics, Faculty of Sciences, Annaba University, BP 12-23000 Annaba, Algeria
(Received 16 September 2015; published 28 March 2016)

A novel scenario for the emergence of geometry in random multitrace matrix models of a single Hermitian matrix M with unitary $U(N)$ invariance, i.e. without a kinetic term, is presented. In particular, the dimension of the emergent geometry is determined from the critical exponents of the disorder-to-uniform-ordered transition, whereas the metric is determined from the Wigner semicircle law behavior of the eigenvalues distribution of the matrix M. If the uniform ordered phase is not sustained in the phase diagram, then there is no emergent geometry in the multitrace matrix model.

I. INTRODUCTION AND MOTIVATION

The original motivation for this work is the theory of noncommutative Φ^4, which we now briefly describe. A scalar phi-four theory on a nondegenerate noncommutative Euclidean spacetime is a three-parameter matrix model of the generic form

$$S = \text{Tr}_H(aM\Delta M + bM^2 + cM^4). \qquad (1.1)$$

The Laplacian Δ captures precisely the underlying geometry, i.e. the metric, of the noncommutative Euclidean spacetime in the sense of [1,2]. This theory can be regularized nonperturbatively using $N \times N$ matrices in an almost obvious way; i.e. the Hilbert space H can be taken to be finite dimensional of size N. This theory exhibits the following three known phases:

(i) The usual second order Ising phase transition between disordered $\langle M \rangle = 0$ and uniform ordered $\langle M \rangle \sim \mathbf{1}_N$ phases. This appears for small values of c. This is the only transition observed in commutative phi-four, and thus it can be accessed in a small noncommutativity parameter expansion.

(ii) A matrix transition between disordered $\langle M \rangle = 0$ and nonuniform ordered $\langle M \rangle \sim \gamma$ phases with $\gamma^2 = \mathbf{1}_N$. This transition coincides, for very large values of c, with the third order transition of the real quartic matrix model, i.e. the model with $a = 0$, which occurs at $b = -2\sqrt{Nc}$. In terms of $\tilde{b} = bN^{-3/2}$ and $\tilde{c} = cN^{-2}$ this reads

$$\tilde{b} = -2\sqrt{\tilde{c}}. \qquad (1.2)$$

This is therefore a transition from a one-cut (disk) phase to a two-cut (annulus) phase [3,4]. See also [5,6].

(iii) A transition between uniform ordered $\langle M \rangle \sim \mathbf{1}_N$ and nonuniform ordered $\langle M \rangle \sim \gamma$ phases. The nonuniform phase, in which translational/rotational invariance is spontaneously broken, is absent in the commutative theory. The nonuniform phase is essentially the stripe phase observed originally on Moyal-Weyl spaces in [7,8].

Thus, the uniform ordered phase $\langle \Phi \rangle \sim \mathbf{1}_N$ is stable in the theory (1.1). This fact is in contrast with the case of the real quartic matrix model $V = \text{Tr}_H(bM^2 + cM^4)$ in which this solution becomes unstable for all values of the couplings. The source of this stability is obviously the addition of the kinetic term to the action.

The nonuniform ordered phase [9] is a full blown nonperturbative manifestation of the perturbative UV-IR mixing effect [10], which is due to the underlying highly nonlocal matrix degrees of freedom of the noncommutative scalar field.

The above picture of the phase diagram holds for noncommutative phi-four in any dimension, and the three phases are all stable and are expected to meet at a triple point. The phase structure in four dimensions was discussed using the Hartree-Fock approximation in [7] and studied by means of the Monte Carlo method, employing the fuzzy torus [11] as regulator, in [8].

In two dimensions the noncommutative phi-four theory is renormalizable [12]. The regularized theory on the fuzzy sphere [13,14] is given by the action (1.1) with a finite dimensional Hilbert space H of size N and a Laplacian $\Delta = [L_a, [L_a, ...]]$ where L_a are the generators of $SU(2)$ in the irreducible representation of spin $(N-1)/2$.

The above phase structure was confirmed in two dimensions by means of Monte Carlo simulations on the fuzzy sphere in [15,16]. Indeed, fuzzy scalar phi-four theory enjoys three stable phases: (i) disordered (symmetric, one-cut, disk) phase; (ii) uniform ordered (Ising, broken, asymmetric one-cut) phase; and (iii) nonuniform ordered (matrix, stripe, two-cut, annulus) phase. The phase diagram is shown on the two graphs of Fig. 1, which were generated using the Metropolis algorithm.

The problem of the phase structure of fuzzy phi-four was also studied by means of the Monte Carlo method in
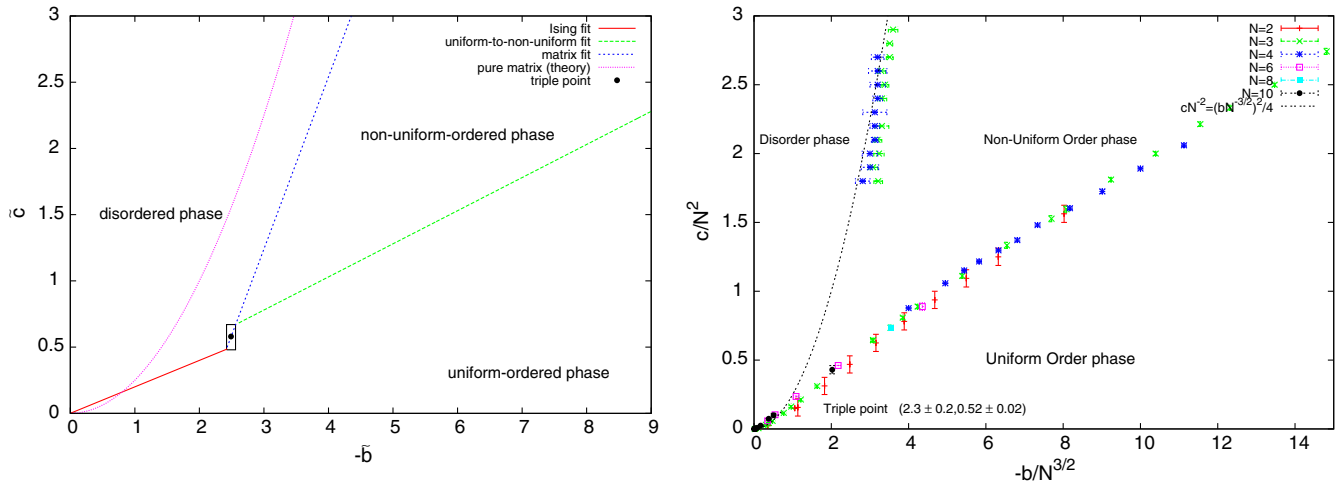
[*]ydri@stp.dias.ie

065055-1

FIG. 1. The phase diagram of noncommutative phi-four theory on the fuzzy sphere. In the first figure the fits are reproduced from actual Monte Carlo data [17]. Second figure reproduced from [15] with the gracious permission of D. O'Connor.

[17–21]. The analytic derivation of the phase diagram of noncommutative phi-four on the fuzzy sphere was attempted in [22–29].

The related problem of Monte Carlo simulation of noncommutative phi-four on the fuzzy torus and the fuzzy disk was considered in [8,30,31], respectively. For a recent study see [32].

In [17] the phase diagram of fuzzy phi-four theory was computed by Monte Carlo sampling of the eigenvalues λ_i of the scalar field M. This was possible by coupling the scalar field M to a $U(1)$ gauge field X_a on the fuzzy sphere, which then allowed us, by employing the $U(N)$ gauge symmetry, to reduce scalar phi-four theory to only its eigenvalues. The pure gauge term is such that the gauge field X_a is fluctuating around $X_a = L_a$.

Another powerful method that allows us to reduce noncommutative scalar phi-four theory to only its eigenvalues, without the additional dynamical gauge field, is the multitrace approach. The multitrace approach was initiated in [22,23]. See also [28] for a review and an extension of this method to the noncommutative Moyal-Weyl plane. For an earlier approach see [29], and for a similar more nonperturbative approach see [24–27]. The multitrace expansion is the analogue of the Hopping parameter expansion on the lattice in the sense that we perform a small kinetic term expansion, i.e. expanding in the parameter a of (1.1), while treating the potential exactly. This should be contrasted with the small interaction expansion of the usual perturbation theory. The effective action obtained in this approach is a matrix model that can be expressed solely in terms of the eigenvalues λ_i and which, on general grounds, can only be a function of the combinations $T_{2n} \propto \sum_{i \neq j}(\lambda_i - \lambda_j)^{2n}$. To the lowest nontrivial order we get an effective action of the form [23,24,28]

$$
S_{\mathrm{eff}} = \sum_i (b\lambda_i^2 + c\lambda_i^4) - \frac{1}{2}\sum_{i \neq j} \ln(\lambda_i - \lambda_j)^2
$$
$$
+ \left[\frac{aN}{4} v_{2,1} \sum_{i \neq j}(\lambda_i - \lambda_j)^2 + \frac{a^2 N^2}{12} v_{4,1}\sum_{i \neq j}(\lambda_i - \lambda_j)^4 \right.
$$
$$
\left. - \frac{a^2}{6} v_{2,2}\left[\sum_{i \neq j}(\lambda_i - \lambda_j)^2\right]^2 + \dots \right]. \qquad (1.3)
$$

The logarithmic potential arises from the Vandermonde determinant, i.e. from diagonalization. The coefficients $v_{2,1}$, $v_{4,1}$, and $v_{2,2}$ are given by $v_{2,1} = +1$, $v_{4,1} = 0$, and $v_{2,2} = 1/8$. Furthermore, it is not difficult to convince ourselves that the above action is a multitrace matrix model since it can be expressed in terms of various moments $m_n = \mathrm{Tr}M^n$ of the matrix M.

The original multitrace matrix model written down [22] comes with different values of v's, and therefore, in the commutative limit $N \to \infty$, it corresponds to a phi-four theory on the sphere modulo multi-integral terms.

Since these multitrace matrix models depend only on N independent eigenvalues, their Monte Carlo sampling by means of the Metropolis algorithm does not suffer from any ergodic problem. The phase diagrams of these models obtained in Monte Carlo simulations will be reported elsewhere.

The remainder of this article is organized as follows:
(1) Section 2: We describe our proposal for how fuzzy geometry can emerge in generic multitrace matrix models.
(2) Section 3: We apply our proposal to an explicit example. We will show that if the multitrace matrix model under consideration does not sustain the uniform ordered phase, then there is no emergent geometry. On the other hand, if the uniform ordered

phase is sustained, then there is an underlying or emergent geometry. In particular, we will show

(i) how to determine the dimension from the critical exponents of the uniform-to-disordered (Ising) phase transition, and

(ii) how to determine the metric (Laplacian, propagator) from the Wigner semicircle law behavior of the eigenvalues distribution of the matrix M.

(3) Section 4: We conclude by giving a straightforward generalization to fuzzy $\mathbf{CP}^n$ and fuzzy $\mathbf{T}^n$.

II. THE PROPOSAL

We start with a general multitrace matrix model rewritten in terms of the moments $\mathrm{Tr}M^n$ with generic parameters $B, C, D, B', C', D', A', \ldots$ as

$$V = B\mathrm{Tr}M^2 + C\mathrm{Tr}M^4 + D[\mathrm{Tr}M^2]^2 + B'(\mathrm{Tr}M)^2$$
$$+ C'\mathrm{Tr}M\mathrm{Tr}M^3 + D'(\mathrm{Tr}M)^4 + A'\mathrm{Tr}M^2(\mathrm{Tr}M)^2 + \cdots. \tag{2.1}$$

This action includes the noncommutative phi-four model on the fuzzy sphere (1.3) and the multitrace matrix model of [22] as special cases. It also includes as special cases the multitrace matrix models obtained by expanding the kinetic term on (i) fuzzy $\mathbf{CP}^n$ [23,33], on (ii) Moyal-Weyl spaces with and without the harmonic oscillator term [28], and on (iii) fuzzy tori [11].

The phase diagram of the action (2.1) will generically contain the matrix one-cut-to-two-cut transition line separating the two stable phases of disorder and nonuniform order. However, the uniform ordered phase will typically be unstable as in the case of the real quartic matrix model

$$V = B\mathrm{Tr}M^2 + C\mathrm{Tr}M^4. \tag{2.2}$$

Our proposal goes as follows. We can check for a possible emergence of geometry in the multitrace matrix model (2.1) by following the three steps:

(1) We compute the phase diagram of the model (2.1). If the uniform ordered phase remains unstable as in the case of the real quartic matrix model (2.2), then there is no geometry and the model is just a trivial deformation of (2.2). In the opposite case we claim that there is an underlying, i.e. emergent, geometry with a well defined dimension (step 2) and a well defined Laplacian/metric (step 3). This means that we can rewrite the multitrace matrix model, in the region of the phase diagram where the uniform ordered phase exists, in terms of a scalar function and a star product with a noncommutativity parameter θ by finding the appropriate Weyl map. As a consequence, a small noncommutativity parameter expansion can be performed and the limit $\theta \to 0$ can be taken. The disordered-to-uniform-ordered phase

transition reduces therefore to the usual second order Ising phase transition on the underlying geometry.

(2) We compute the dimension of the underlying by computing the critical exponents of the disordered-to-uniform-ordered phase transition, which, by universality, take specific values in each dimension.

(3) We compute the Laplacian by computing the free behavior of the propagator. This is done explicitly by computing the eigenvalues distribution of the matrix M in the free regime, small values of C, and comparing with the Wigner semicircle law behavior, which must hold with a specific radius depending crucially on the kinetic term.

III. EXPLICIT EXAMPLE: THE FUZZY SPHERE

A. Phase diagram

We consider as an example the multitrace matrix model of [22] which comes with the v values $v_{2,1} = -1$, $v_{4,1} = 3/2$, and $v_{2,2} = 0$. The action is given explicitly by

$$V = B\mathrm{Tr}M^2 + C\mathrm{Tr}M^4 + D[\mathrm{Tr}M^2]^2 + B'(\mathrm{Tr}M)^2$$
$$+ C'\mathrm{Tr}M\mathrm{Tr}M^3. \tag{3.1}$$

The parameters D, B', and C' are constrained as $D = 3N/4$, $B' = \sqrt{N}/2$, and $C' = -N$. The phase diagram of this model is computed by means of Monte Carlo simulation elsewhere. The result is shown in Fig. 2. The details of the corresponding nontrivial lengthy Monte Carlo calculation will be reported elsewhere. As desired we have three stables phases in this particular model meeting at a triple point. In other words, we have established that this multitrace matrix model sustains the uniform ordered phase, which is the first requirement.

B. Dimension from critical exponents

The uniform ordered phase is also called the Ising phase precisely because we believe that the corresponding transition to the disordered phase is characterized by the universal critical exponents of the Ising model in two dimensions derived from the Onsager solution. These critical exponents are defined as usual by the following behavior:

$$m/N = \langle|\mathrm{Tr}M|\rangle/N \sim (B_c - B)^\beta \sim N^{-\beta/\nu},$$
$$C_v/N^2 \sim (B - B_c)^{-\alpha} \sim N^{\alpha/\nu},$$
$$\chi = \langle|\mathrm{Tr}M|^2\rangle - \langle|\mathrm{Tr}M|\rangle^2 \sim (B - B_c)^{-\gamma} \sim N^{\gamma/\nu} \sim N^{2-\eta},$$
$$\xi \sim |B - B_c|^{-\nu} \sim N. \tag{3.2}$$

There are in total six critical exponents, the above five plus the critical exponent δ that controls the equation of state, but only two are truly independent because of the so-called scaling laws. The Onsager solution of the Ising model in two dimensions gives the following celebrated values [34]:
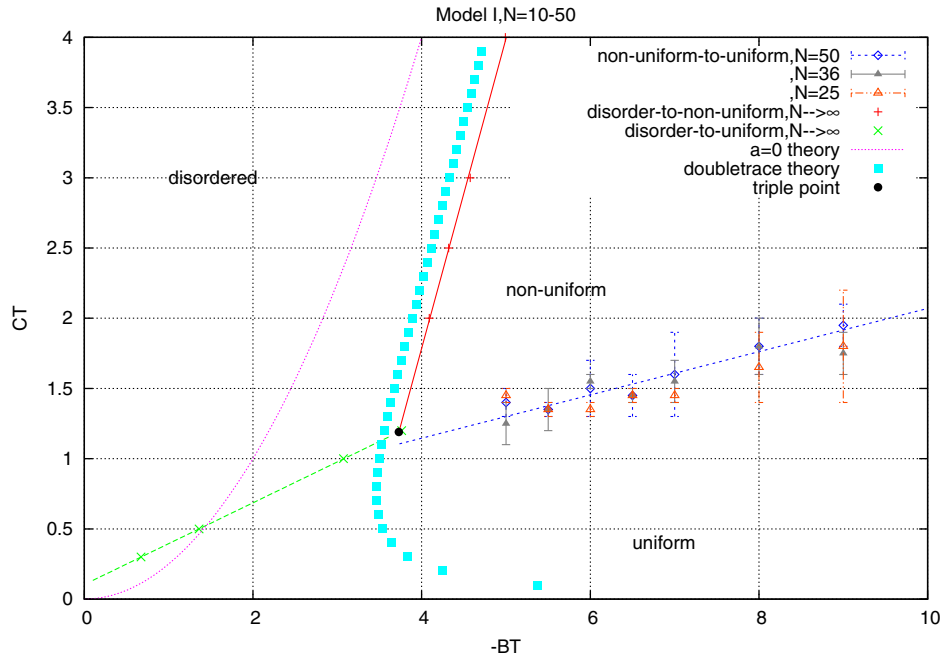
FIG. 2. The phase diagram of the multitrace matrix model of [22]. The Ising and matrix transition data points are not shown but we only indicate their extrapolated fits, whereas the $N = 25$, $N = 36$, and $N = 50$ stripe data points are included explicitly.

$$\nu = 1, \qquad \beta = 1/8, \qquad \gamma = 7/4,$$
$$\alpha = 0, \qquad \eta = 1/4, \qquad \delta = 15. \qquad (3.3)$$

This fundamental result is very delicate to check explicitly in the Monte Carlo data. Since we must necessarily deal with the critical region, we must face the two famous problems of finite size effects and critical slowing down. In this particular problem, the critical slowing down problem can be shown to start appearing in Monte Carlo simulations around $N > 60$ so we will keep below this value and employ very large statistics of the order of 2^{20} to avoid it. A more systematic solution to this problem is to employ the Wolf algorithm [35], which we do not attempt here. We simply employ here the ordinary Metropolis algorithm. The problem of finite size effects is also very serious for the measurement of the critical exponents since the above behavior (3.2) is supposed to hold only for large N. This problem can be avoided by not including values of N less than 20, and thus below we will quote for completeness $N = 10$ and $N = 15$ data but, in most cases, we will not take them into account in the fitting.

Since the Ising model appears from the Φ^4 theory for large values of the quartic coupling, it is preferable to use values of $\tilde{C}$ as large as possible. However, we are limited from above by the appearance of the different physics of the transition between the disordered and nonuniform-ordered phases around $\tilde{C} = 1.5$. Thus, we choose $\tilde{C} = 1.0$, which is relatively large but well established to be within the Ising transition with an extrapolated critical point around $\tilde{B} = -3.07$ (see below). The critical behavior of the

magnetization, susceptibility, and specific heat around the critical value of $\tilde{B} = -3.10$ is shown in Fig. 3. We attach in Table I some data relevant for the computation of the critical exponents ν, β, γ, and α. The other critical exponents can be determined via scaling laws.

The measurements of the critical exponents ν, β, γ, and α proceed as follows:

(i) *Critical point and the critical exponent ν*: By plotting the critical point $\tilde{B}_c$ obtained for each N versus N (first and second columns of Table I) we get immediately both the $N = \infty$ critical point and the critical exponent ν. We obtain (see Fig. 5 below)

$$\tilde{B}_c = -1.061(168) \cdot N^{-0.926(83)} - 3.074(6) \Rightarrow,$$
$$\nu = 0.926(83). \qquad (3.4)$$

Also we obtain

$$\tilde{B}_* = -3.074(6). \qquad (3.5)$$

This prediction for ν agrees reasonably well with the Onsager calculation. In the following we will assume for simplicity that $\nu = 1$. The above fit is the only instance in which we have included $N = 10$ and $N = 15$, and thus we believe that the obtained value of $-\tilde{B}_*$ is an underestimation of the true critical point.

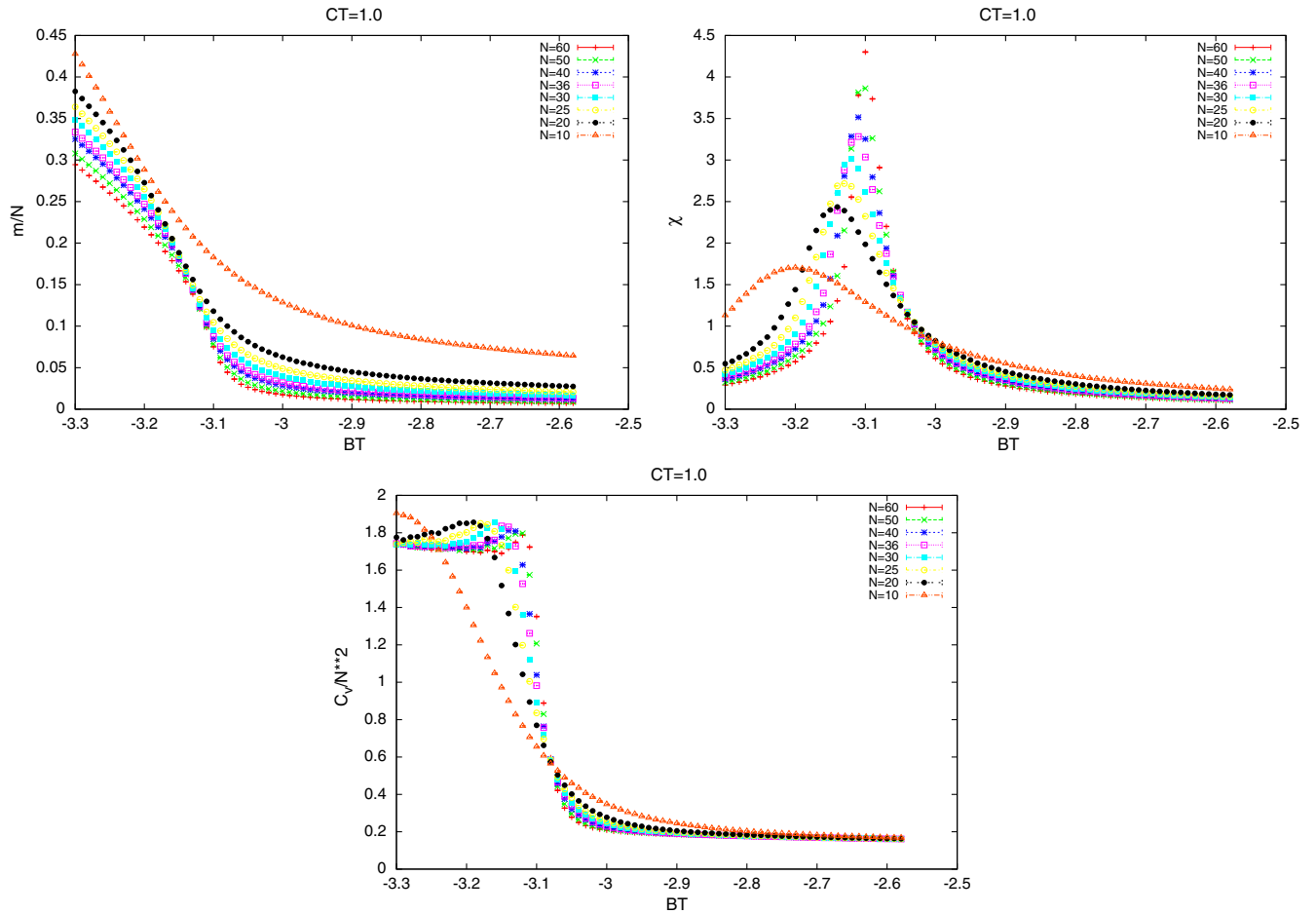(ii) *Magnetization and the critical exponent β*: The magnetization and the zero power are defined by

FIG. 3. The Ising critical behavior.

$$m = \langle |\mathrm{Tr}M| \rangle, \quad \chi = \langle |\mathrm{Tr}M|^2 \rangle - \langle |\mathrm{Tr}M| \rangle^2. \quad (3.6)$$

$$P_0 = \left\langle \left(\frac{1}{N} \mathrm{Tr}M \right)^2 \right\rangle. \quad (3.7)$$

Measurements of the magnetization m/N were performed near the extrapolated critical point $\tilde{B} = -3.07$

for $\tilde{C} = 1.0$ but inside the uniform ordered phase. These are then used to compute the critical exponent β by searching for a power law behavior.

More precisely, we measure $\ln(m/N)$ versus $\ln N$ for each value of $\tilde{B}$ very near and around $\tilde{B} = -3.10$, fit to a straight line in the range $20 \leq N \leq 60$, compute the slope β, and then search for the flattest

TABLE I. Measurements of the magnetization $(m/N)_{<*}$, the susceptibility $\chi_{<*}$ via the zero power $(P_0)_{<*}$, and the specific heat $(C_v/N^2)_*$ used to compute the critical exponents β, γ, and α, respectively. Here $\tilde{C} = 1.0$, the extrapolated critical point is $\tilde{B} = -3.07$, the critical point as the intersection point of curves of specific heat is $\tilde{B} = -3.08$, and the critical point as the flattest line of decrease of magnetization is $\tilde{B} = -3.13$.

| N	$\tilde{B}_c, \tilde{B}_* = -3.07$	χ_c	$(C_v)_*, \tilde{B}_* = -3.08$	$\tilde{B} < \tilde{B}_* = -3.13$	$m_{<*}$	$10^3 (P_0)_{<*}$
10	-3.20	1.704(2)	56.467(94)	-3.14	2.1776(12)	6.256(6)
15	-3.16	2.089(2)	129.111(217)	-3.14	2.7750(14)	4.315(4)
20	-3.14	2.436(3)	229.861(389)	-3.14	3.4423(15)	3.571(2)
25	-3.13	2.716(3)	365.183(621)	-3.14	4.1759(16)	3.220(2)
30	-3.12	3.017(4)	524.253(891)	-3.14	4.9772(16)	3.042(2)
36	-3.11	3.283(4)	749.099(1267)	-3.14	5.8878(15)	2.860(1)
40	-3.11	3.515(4)	941.139(1607)	-3.14	6.5134(14)	2.782(1)
50	-3.10	3.864(4)	1461.597(2479)	-3.14	7.9250(12)	2.576(1)
60	-3.10	4.301(5)	2144.929(3658)	-3.14	9.2021(11)	2.388(1)
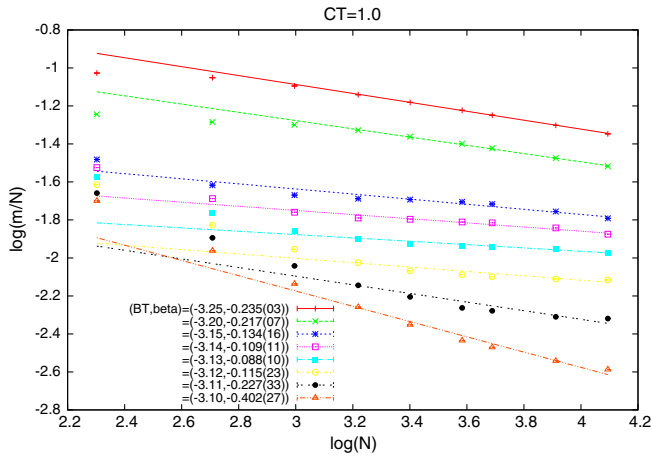
FIG. 4. The critical exponent β.

line, i.e. the smallest slope β. This value marks the transition from the Ising phase to the disordered phase. Deep inside the Ising phase the slope should approach the mean field value $-1/4$, which can be shown from the scaling behavior of the dominant configuration. After determining the critical value we

then consider the value of $\tilde{B}$ nearest to it but within the Ising phase and take the slope there to be the value of the critical exponent β. In our example here, the flattest line occurs at $\tilde{B} = -3.13$ with slope $-0.088(10)$ after which the slope becomes $-0.109(11)$ at $\tilde{B} = -3.14$. The slope goes fast to the mean field value -0.25 as we keep decreasing $\tilde{B}$. See Fig. 4. Our measured value of the critical point $\tilde{B}_*$ from the magnetization and of the critical exponent β are therefore

$$\tilde{B}_* = -3.13, \tag{3.8}$$

$$\ln\frac{m}{N} = -0.109(11) \cdot \ln N - 1.423(43)$$

$$\Rightarrow \beta = -0.109(11). \tag{3.9}$$

(iii) *Susceptibility and zero power and the critical exponent* γ: The measurement of the critical exponent γ is quite delicate and will be done indirectly as follows. We rewrite the susceptibility in terms of the zero power and magnetization as
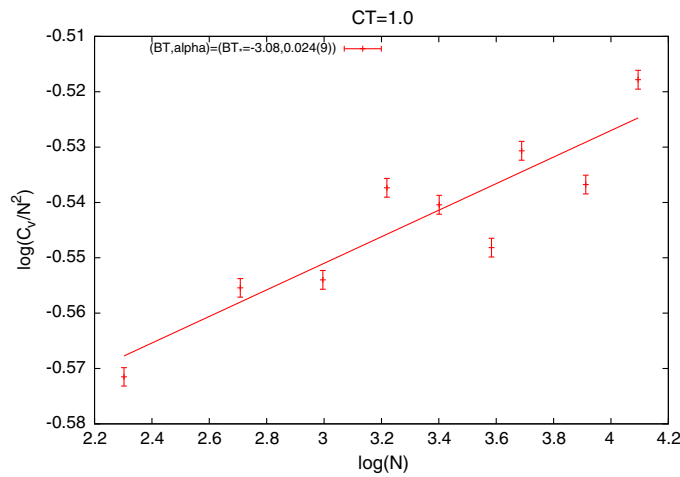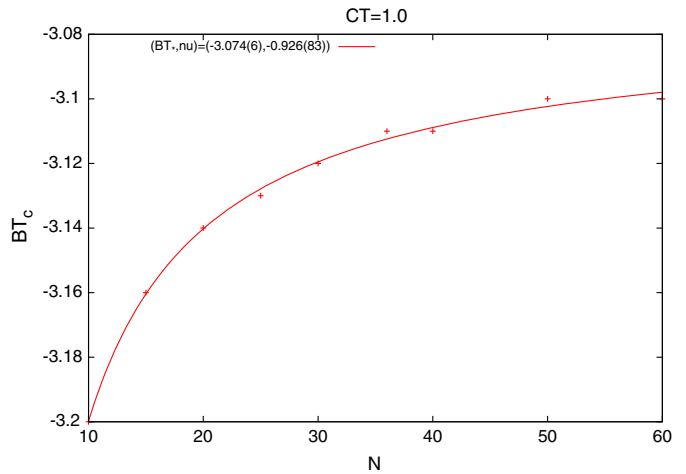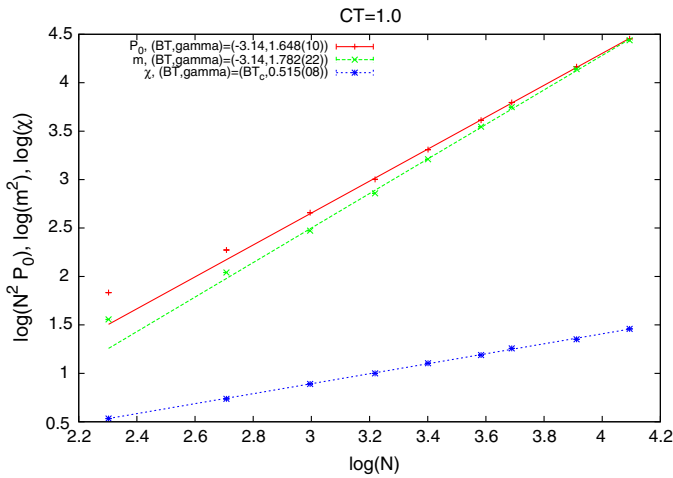

FIG. 5. The critical exponents ν, γ, and α.

$$\chi = \langle|\mathrm{Tr}M|^2\rangle - \langle|\mathrm{Tr}M|\rangle^2 = N^2 P_0 - m^2. \qquad (3.10)$$

The critical exponent γ in terms of the critical exponent γ' of P_0 is then given by

$$\gamma = 2 + \gamma'. \qquad (3.11)$$

By using the results shown in Table I at $\tilde{B} = -3.14$, plotted in Fig. 5, we obtain the following exponents:

$$\ln P_0 = -0.352(10) \cdot \ln N - 2.289(36)$$
$$\Rightarrow \gamma' = -0.352(10). \qquad (3.12)$$

Or equivalently

$$\ln N^2 P_0 = 1.648(10) \cdot \ln N - 2.289(36)$$
$$\Rightarrow \gamma = 1.648(10). \qquad (3.13)$$

For consistency we can check that the second term in the susceptibility behaves using the result (3.9) as

$$\ln m^2 = 1.782(22) \cdot \ln N - 2.846(86)$$
$$\Rightarrow \gamma = 1.782(22). \qquad (3.14)$$

Our two measurements of the critical exponent γ agree reasonably well with the Onsager values.

If we try to fit the values of the susceptibility at its maximum shown in the third column of Table I, i.e. at the peak that keeps slowly moving with $\tilde{B}$, then we will obtain a very bad underestimate of the critical exponent γ given by

$$\ln \chi_{\max} = 0.515(08) \cdot \ln N - 0.652(30)$$
$$\Rightarrow \gamma = 0.515(08). \qquad (3.15)$$

This in our mind is due in part to the dependence of $\tilde{B}_c$ on N and in another part is an indication of the critical slowing down problem showing up in the measurement of this second moment; i.e. the size of the fluctuations is observed to grow with N at the critical point but not at the correct rate indicated by the independent measurements of the zero moment and the magnetization. See Fig. 5.

(iv) *Specific heat and the critical exponent α*: The specific heat is defined by

$$C_v = \langle S^2 \rangle - \langle S \rangle^2. \qquad (3.16)$$

The critical point $\tilde{B}_*$ as measured from the specific heat is identified by the intersection point of the various curves with different N shown in Fig. 3. We get

$$\tilde{B}_* = -3.08. \qquad (3.17)$$

This measurement is contrasted very favorably with the independent measurement obtained from the extrapolated value of $\tilde{B}_c$ shown in Eq. (3.5) but should also be contrasted with the measurement obtained from the magnetization shown in Eq. (3.8).

By using the results shown in Table I at the critical point $\tilde{B} = -3.08$, plotted in Fig. 5, we obtain the following exponent:

$$\ln \frac{C_v}{N^2} = 0.024(9) \cdot \ln N - 0.623(31)$$
$$\Rightarrow \alpha = 0.024(9). \qquad (3.18)$$

C. Free propagator from Wigner semicircle law

We can also measure the emergent geometry by measuring the free propagator of the theory. This will give us information on both the dimension and the metric since the free propagator is the inverse of the Laplacian Δ that fully encodes the underlying geometry in the sense of [1,2]. This goes as follows [29].

A noncommutative phi-four on a d-dimensional noncommutative Euclidean spacetime $\mathbf{R}_\theta^d$ reads in position representation

$$S = \int d^d x \left(\frac{1}{2}\partial_i\Phi\partial_i\Phi + \frac{1}{2}m^2\Phi^2 + \frac{\lambda}{4}\Phi_*^4\right). \qquad (3.19)$$

The first step is to regularize this theory in terms of a finite $\mathcal{N}$-dimensional matrix Φ and rewrite the theory in matrix representation. Then we diagonalize the matrix Φ. The measure becomes $\int \prod_i d\Phi_i \Delta^2(\Phi) \int dU$ where Φ_i are the eigenvalues, $\Delta^2(\Phi) = \prod_{i<j}(\Phi_i - \Phi_j)^2$ is the Vandermonde determinant, and dU is the Haar measure. The effective probability distribution of the eigenvalues Φ_i can be determined uniquely from the behavior of the expectation values $\langle \int d^d x \Phi_*^{2n}(x)\rangle$. These objects clearly depend only on the eigenvalues Φ_i and are computed using a sharp UV cutoff Λ. If we are only interested in the eigenvalues of the scalar matrix Φ, then the free theory $\lambda = 0$ can be replaced by the effective matrix model [29]

$$S = \frac{2\mathcal{N}}{\alpha_0^2}\mathrm{Tr}\Phi^2. \qquad (3.20)$$

This result can be traced to the fact that planar diagrams dominate over the nonplanar ones in the limit $\Lambda \to \infty$. This means in particular that the eigenvalues Φ_i are distributed according to the famous Wigner semicircle law with α_0 being the largest eigenvalue, viz.

$$\rho(t) = \frac{2}{\pi \alpha_0^2} \sqrt{\alpha_0^2 - t^2}, \qquad -\alpha_0 \leq t \leq +\alpha_0. \qquad (3.21)$$

In the most important cases of $d = 2$ and $d = 4$ dimensions we have explicitly

$$\alpha_0^2(m, \Lambda) = \frac{1}{4\pi^2} \left(\Lambda^2 - m^2 \ln\left(1 + \frac{\Lambda^2}{m^2}\right) \right), \quad d = 4, \quad (3.22)$$

$$\alpha_0^2(m, \Lambda) = \frac{1}{\pi} \ln\left(1 + \frac{\Lambda^2}{m^2}\right), \qquad d = 2. \qquad (3.23)$$

Obviously, dimension four is eliminated by the results of the critical exponents. In two dimensions the regulator Λ originates in only one of two possible noncommutative spaces [29]:

(1) *Fuzzy torus:* As it turns the results on the fuzzy torus are different from those obtained using a sharp momentum cutoff due to the different behavior of the propagator for large momenta, and as a consequence the resulting formula for α_0^2 is different from the above Eq. (3.23). We obtain instead

$$\alpha_0^2(m, \Lambda) = 4 \int_0^\pi \frac{d^2 r}{(2\pi)^2} \frac{1}{\sum_i (1 - \cos r_i) + m^2 l^2 / 2},$$
$$d = 2. \qquad (3.24)$$

l here is the lattice spacing, the noncommutativity is quantized as $\theta = N l^2 / \pi$, and the cutoff is

$$\Lambda = \frac{\pi}{l} = \sqrt{\frac{N\pi}{\theta}}. \qquad (3.25)$$

The above behavior can easily be excluded in our Monte Carlo data, and by hindsight we know that this should be so indeed because the original multitrace approximation is relevant to the fuzzy sphere.

(2) *Fuzzy sphere:* The fuzzy sphere $\mathbf{S}_N^2 = \mathbf{CP}_N^1$ is the simplest of fuzzy projective spaces $\mathbf{CP}_N^n$. In this case $\mathcal{N} = N + 1$ and the scalar field Φ becomes an $N \times N$ matrix ϕ given by $\phi = \sqrt{2\pi/Na}\Phi$. In this case the cutoff is given in terms of the matrix size N and the radius R of the sphere by

$$\Lambda = \frac{N}{R}. \qquad (3.26)$$

Also, in this case the mass parameters B and m^2 are related by

$$m^2 = \frac{b}{aR^2}. \qquad (3.27)$$

By using $\tilde{B} = B/N^{3/2}$ and choosing $a = 2\pi/N$, so that $\Phi = \phi$, we obtain

$$\frac{\Lambda^2}{m^2} = \frac{2\pi}{\sqrt{N}\tilde{B}}. \qquad (3.28)$$

We get then

$$\alpha_0^2(m, \Lambda) = \frac{1}{\pi} \ln\left(1 + \frac{2\pi}{\sqrt{N}\tilde{B}}\right). \qquad (3.29)$$

In the limit $B \to \infty$ we get the one-cut $\delta^2 = 2N/B$ of the Gaussian matrix model $B\mathrm{Tr}M^2$, viz. $B = 2\mathcal{N}/\alpha_0^2$. This can also be obtained by taking the limit $B \to \infty$ of the one-cut (deformed Wigner semicircle law) solution

$$\rho(\lambda) = \frac{1}{N\pi} (2C\lambda^2 + B + C\delta^2) \sqrt{\delta^2 - \lambda^2},$$
$$\delta^2 = \frac{1}{3C}(-B + \sqrt{B^2 + 12NC}) \qquad (3.30)$$

of the quadratic matrix model $B\mathrm{Tr}M^2 + C\mathrm{Tr}M^4$.

This result was also generalized in [26]. The eigenvalues distribution of a free scalar field theory on the fuzzy sphere with an arbitrary kinetic term, viz. $S = \mathrm{Tr}(M\mathcal{K}M + BM^2)/2$, where $\mathcal{K}(0) = 0$ and $\mathcal{K}$ is diagonal in the basis of polarization tensors T_m^l, is always given by a Wigner semicircle law with a radius

$$R^2 = \delta^2 = \alpha_0^2 = \frac{4f(B)}{N},$$
$$f(B) = \sum_{l=0}^{N-1} \frac{2l + 1}{\mathcal{K}(l) + B}. \qquad (3.31)$$

Some Monte Carlo results are shown in Figs. 6 and 7. These are obtained in Monte Carlo runs with 2^{20} thermalization steps and 2^{18} thermalized configurations where each two configurations are separated by 2^4 Monte Carlo steps in order to reduce autocorrelation effects. We consider $N = 20 - 40$, $\tilde{C} = 0.05 - 0.35$, and $\tilde{B} = 0 - 5$.

It is not difficult to convince ourselves that the mass parameter B is precisely the mass squared in this regime. For each value of $(N, \tilde{C}, \tilde{B})$ we compute the eigenvalues distribution $\rho(\lambda)$ and fit it to the Wigner semicircle law (3.21) (see Fig. 6). We obtain thus a measurement of the radius of the Wigner semicircle law $\delta^2 = \alpha_0^2 = R^2$. We have checked carefully that in this regime the Wigner semicircle law is the appropriate behavior rather than the one-cut solution (3.30) as evidenced by the first graph in Fig. 6. The measurement of the radii δ^2 for various values of $\tilde{B}$ is then plotted and compared with the expected theoretical behaviors (3.29) as well as with the $B \to \infty$
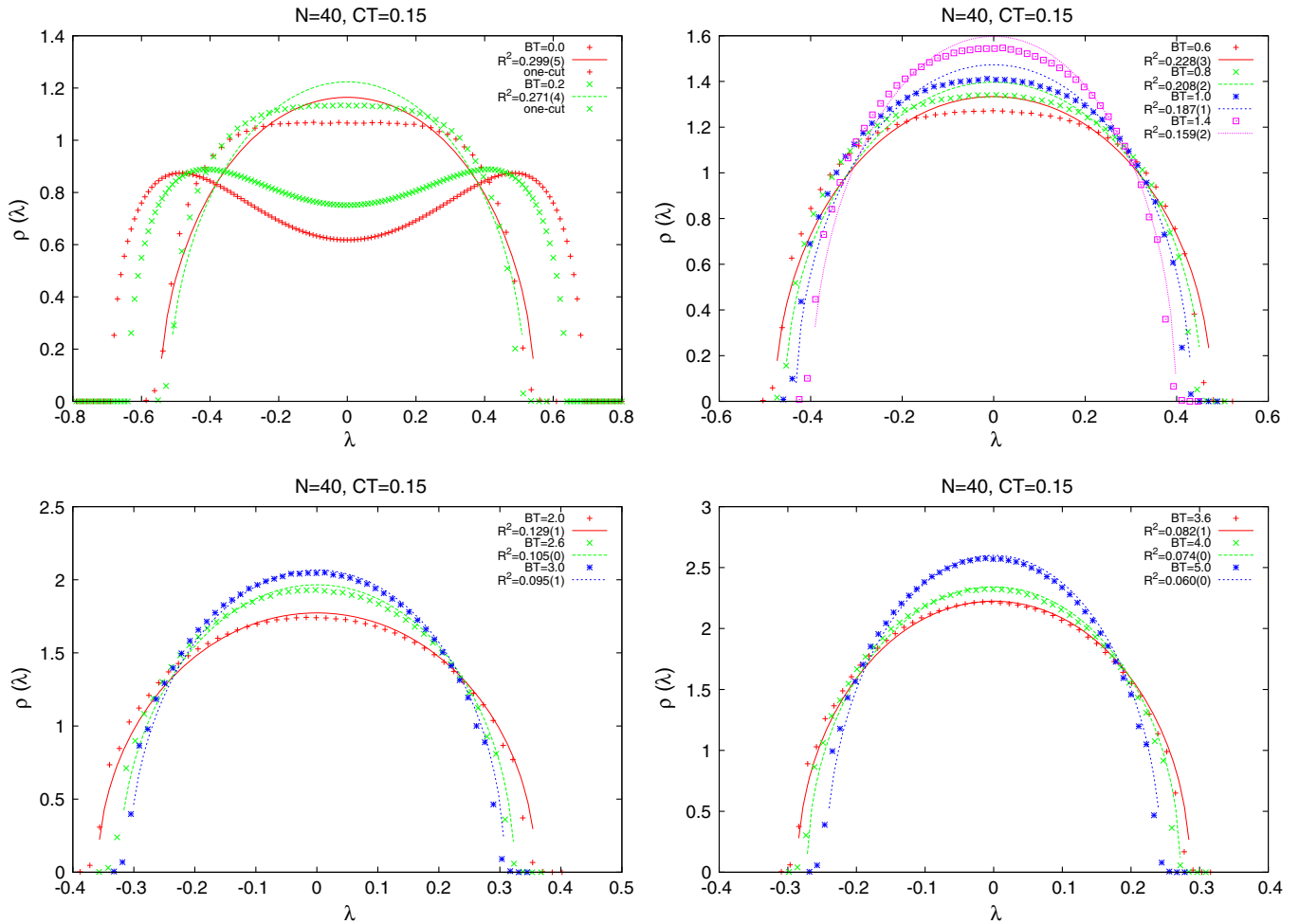
FIG. 6.   The semicircle law as a function of $\tilde{B}$.

behavior $\delta^2 = 2N/B$ (see Fig. 7). The agreement with (3.29) is very reasonable with some deviation for small values of $\tilde{B}$ as we approach the nonperturbative region where the uniform ordered phase appears at some $\tilde{B} < 0$.

This discrepancy for small values of $\tilde{B}$ is already seen in Fig. 6 when we fit the distributions to the Wigner semicircle law. However, this effect is reduced as we decrease the value of $\tilde{C}$.
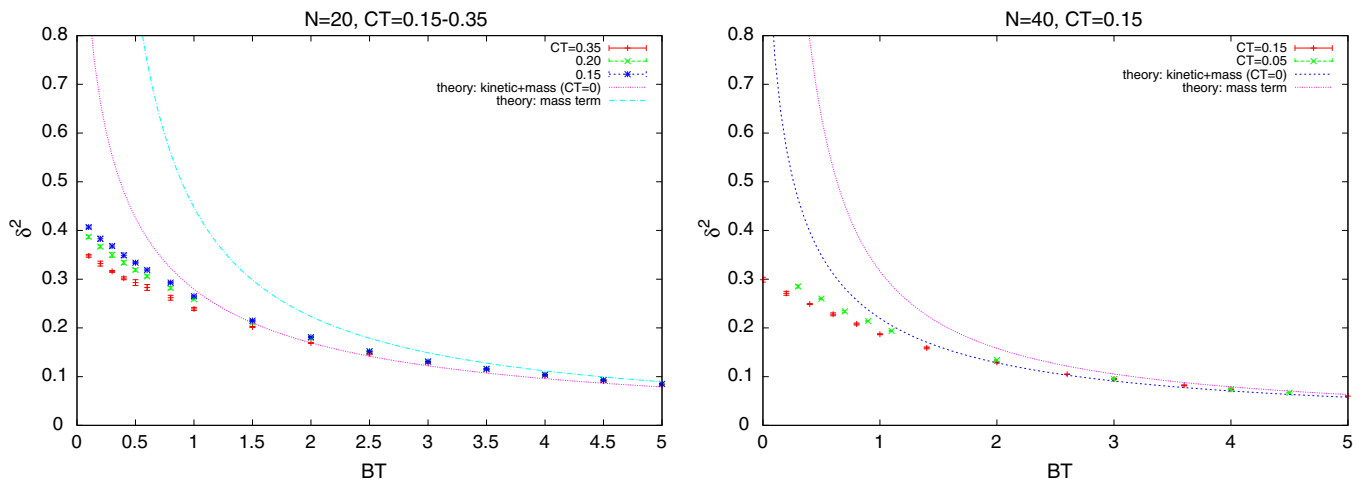

FIG. 7.   The behavior of the radius of the Wigner semicircle law $\delta^2 = \alpha_0^2$ as a function of $\tilde{B}$.

In summary we conclude that we are indeed dealing with the geometry of the fuzzy sphere and, given hindsight, we know that this should be true.

IV. GENERALIZATION AND CONCLUSION

The emergence of geometry in the very early universe is a problem of fundamental importance to our understanding of quantum gravity and cosmology. In this article, we have proposed a novel scenario for the emergence of geometry in random multitrace matrix models that depend on a single Hermitian matrix M with full unitary $U(N)$ invariance and without any kinetic term. Thus, the model under consideration has no geometry *a priori* precisely because of the absence of a kinetic term. On the other hand, previous proposals of emergent geometry required the input of several matrices with some rotational symmetry group besides the $U(N)$ gauge symmetry [36].

Our proposal consists in checking whether the uniform ordered phase is sustained by the multitrace matrix model under consideration. If yes, then the dimension of the underlying geometry, in the region of the phase diagram where the uniform ordered phase is stable, can be inferred from the values of the critical exponents of the Ising phase transition, whereas the metric/Laplacian of this geometry can be inferred from the behavior of the free propagator encoded in the Wigner semicircle law behavior of the eigenvalues distribution of the matrix M in the weakly coupled regime. An explicit example is given in which the geometry of the fuzzy sphere emerges, with all the correct properties, in the phase diagram of a particular multitrace matrix model containing multitrace terms depending on the moments $m_1 = \mathrm{Tr}M$, $m_2 = \mathrm{Tr}M^2$, and $m_3 = \mathrm{Tr}M^3$ in a particular way [22].

This idea can be generalized in a straightforward way to all higher fuzzy projective spaces $\mathbf{CP}^n$ and fuzzy tori $\mathbf{T}^n$ by tuning appropriately the coefficients of the multitrace matrix model and/or including higher moments in the multitrace matrix model.

ACKNOWLEDGMENTS

[1] A. Connes, *Noncommutative geometry* (Academic Press, London, 1994).

[2] J. Frohlich and K. Gawedzki, Conformal field theory and geometry of strings, *Proceedings of Mathematical quantum theory, British Columbia, Canada* (1993).

[3] Y. Shimamune, Phys. Lett. **108B,** 407 (1982).

[4] E. Brezin, C. Itzykson, G. Parisi, and J. B. Zuber, Commun. Math. Phys. **59,** 35 (1978).

[5] B. Eynard, Cours de Physique Theorique de Saclay (unpublished).

[6] N. Kawahara, J. Nishimura, and A. Yamaguchi, J. High Energy Phys. 06 (2007) 076.

[7] S. S. Gubser and S. L. Sondhi, Nucl. Phys. B **B605,** 395 (2001).

[8] J. Ambjorn and S. Catterall, Phys. Lett. B **549,** 253 (2002).

[9] S. A. Brazovkii, Zh. Eksp. Teor. Fiz. **68,** 175 (1975).

[10] S. Minwalla, M. Van Raamsdonk, and N. Seiberg, J. High Energy Phys. 02 (2000) 020.

[11] J. Ambjorn, Y. M. Makeenko, J. Nishimura, and R. J. Szabo, J. High Energy Phys. 05 (2000) 023.

[12] H. Grosse and R. Wulkenhaar, J. High Energy Phys. 12 (2003) 019.

[13] J. Hoppe, Ph. D. thesis, MIT, 1982.

[14] J. Madore, Classical Quantum Gravity **9,** 69 (1992).

[15] F. Garcia Flores, X. Martin, and D. O'Connor, Int. J. Mod. Phys. A **24,** 3917 (2009).

[16] F. Garcia Flores, D. O'Connor, and X. Martin, *Proc. Sci.*, LAT2005 (2006) 262 [arXiv:hep-lat/0601012].

[17] B. Ydri, J. High Energy Phys. 03 (2014) 065.

[18] X. Martin, J. High Energy Phys. 04 (2004) 077.

[19] M. Panero, J. High Energy Phys. 05 (2007) 082.

[20] J. Medina, W. Bietenholz, and D. O'Connor, J. High Energy Phys. 04 (2008) 041.

[21] C. R. Das, S. Digal, and T. R. Govindarajan, Mod. Phys. Lett. A **23,** 1781 (2008).

[22] D. O'Connor and C. Saemann, J. High Energy Phys. 08 (2007) 066.

[23] C. Saemann, SIGMA **6,** 050 (2010).

[24] A. P. Polychronakos, Phys. Rev. D **88,** 065010 (2013).

[25] J. Tekel, J. High Energy Phys. 10 (2014) 144.

[26] V. P. Nair, A. P. Polychronakos, and J. Tekel, Phys. Rev. D **85,** 045021 (2012).

[27] J. Tekel, Phys. Rev. D **87,** 085015 (2013).

[28] B. Ydri, arXiv:1410.4881 [Phys. Rev. D (to be published)].

[29] H. Steinacker, J. High Energy Phys. 03 (2005) 075.

[30] W. Bietenholz, F. Hofheinz, and J. Nishimura, J. High Energy Phys. 06 (2004) 042.

[31] F. Lizzi and B. Spisso, Int. J. Mod. Phys. A **27,** 1250137 (2012).

[32] H. Meja-Daz, W. Bietenholz, and M. Panero, J. High Energy Phys. 10 (2014) 56.

[33] A. P. Balachandran, B. P. Dolan, J. H. Lee, X. Martin, and D. O'Connor, J. Geom. Phys. **43,** 184 (2002).

[34] L. Onsager, Phys. Rev. **65,** 117 (1944).

[35] U. Wolff, Phys. Rev. Lett. **62,** 361 (1989).

[36] R. Delgadillo-Blando, D. O'Connor, and B. Ydri, Phys. Rev. Lett. **100,** 201601 (2008).